Long-time self-diffusion in binary colloidal hard-sphere dispersions

A. Imhof and J. K. G. Dhont
Van't Hoff Laboratory for Physical and Colloid Chemistry, Utrecht University, Padualaan 8, 3584 CH Utrecht, The Netherlands
(Received 21 June 1995)

The long-time self-diffusion and phase behavior of a binary dispersion of hard spheres with a size ratio of 1:9.3 were studied. Labeling one of the particle species in the mixtures with a fluorescent dye allows for the measurement of its long-time self-diffusion coefficient using fluorescence recovery after photobleaching. Extensive measurements are reported for a wide range of volume fractions and mixture compositions. For high volume fractions, the data can be described by empirical formulas in which interactions of a tracer with particles of different sizes are effectively decoupled. The binary system shows a fluid-crystal type phase separation. No fluid-fluid phase separation is observed. At high volume fractions, two different glassy states are found. These two states could be distinguished by the separate measurement of the mobility of the small and the large spheres. In one of the glassy states, the small spheres remain mobile although the large spheres are structurally arrested. In the other, both particles are arrested.

PACS number(s): 82.70.Dd, 66.10.−x, 64.70.Dv, 83.10.Pp

I. INTRODUCTION

Among the most striking aspects of the behavior of binary hard-sphere mixtures are superlattice formation at the freezing transition [1,2] and phase separation [3–5]. In order to understand these phenomena, the concept of depletion attraction has been introduced [6,7]. Until now most of the attention has been focused on the static properties of these asymmetric mixtures, and much less is known about their dynamical properties. In this work aspects of both statics and dynamics of a binary colloidal dispersion composed of hard spheres with a size ratio of 1:9.3 are addressed. We previously determined the phase diagram of this mixture [8]. Phase separation into a fluid and a crystalline phase, and two different glass states were found. In this paper, in addition to a discussion of the phase behavior, we present a systematic investigation of the long-time self-diffusion coefficient $D_{s,L}$ of both the small and large spheres for a wide range of volume fractions and mixture compositions.

So far, the study of self-diffusion in dispersions of differently sized particles has mostly been limited to dilute systems of highly charged spheres, in which hydrodynamic interactions are negligible. Moreover, the concentration and composition of the mixtures have not been varied in a systematic way. Most of the earlier experiments used dynamic light scattering (DLS) to measure particle dynamics, and were thereby limited to the analysis of the large particles that scatter most of the light. With this technique, long-time self-diffusion [9], as well as short- and intermediate-time self-diffusion [10,11], have been measured for systems composed of a small number of large charged spheres in a dispersion of many small charged spheres. Also, some measurements have been reported of an effective short-time diffusion coefficient of dense binary hard-sphere dispersions with diffusing wave spectroscopy (DWS) [12]. Finally, with forced Rayleigh scattering (FRS) [13], the long-time self-diffusion coefficients of both particle species in dilute binary dispersion of charged spheres have been obtained.

In this work we use the technique fluorescence recovery after photobleaching (FRAP) to measure $D_{s,L}$ of both particles as a function of concentration and mixture composition. Separate measurement of each particle species is made possible by labeling that component with a fluorescent dye. The fact that FRAP is not reliant on scattering, nor hindered by it, constitutes a considerable advantage over DLS, and in particular allows the study of the small particles' dynamics. FRAP is also better suited to measure the long-time limit and, indeed, very slow diffusion processes are measurable. This is also the most important limitation, namely that short times are not accessible.

The particle dynamics in hard-sphere dispersions are strongly influenced by both direct and hydrodynamic interactions. Theoretical expressions for $D_{s,L}$, given by Batchelor [14], are available to leading order in the volume fractions of the components, and are tested against our results. At higher concentrations, where particle motions become very strongly coupled, no theoretical results are available. Instead, we present an empirical expression that provides a good description of the data. At the highest concentrations glassy states are found, which are evidenced by incomplete decay of the correlation functions that are measured with FRAP, indicating that long-time self-diffusion has effectively stopped. The measurements provide evidence of the existence of two different glassy states which occur in different parts of the phase diagram. In one of these, both particles are frozen in. In the other, however, only the large spheres show structural arrest while the small particles have complete relaxation, though in a nonsingle exponential fashion.

In Sec. II the theoretical background of self-diffusion in colloidal dispersions is briefly described, and the results of Batchelor's theory are applied to the present system. Then in Sec. III details on particle preparation,

characterization, and experimental procedures are given. Results are presented and discussed in Sec. IV, and conclusions are summarized in Sec. V.

II. THEORETICAL BACKGROUND

Brownian motion of colloidal particles is the result of fluctuating forces which these particles experience from collisions with molecules of the medium in which they are suspended. The velocity of a spherical particle fluctuates on a time scale of order $\tau_B = m/6\pi\eta_0 a$, where m is its mass, a its radius, and η_0 the shear viscosity of the solvent. τ_B is called the Brownian time scale. For times longer than τ_B the motion of particles is diffusive. A measure for the diffusive motion of a certain particle (the tracer) is its mean-square displacement $\langle \Delta r^2(t) \rangle$ as a function of time t. For independent particles this is a linear function of time,

$$\langle \Delta r^2(t) \rangle = 6D_0 t \ , \quad t \gg \tau_B \ . \tag{1}$$

Here D_0 is the single particle diffusion coefficient given by the well-known Stokes-Einstein formula

$$D_0 = \frac{kT}{6\pi\eta_0 a} \ , \tag{2}$$

where k is Boltzmann's constant, and T the absolute temperature. When the dispersion is not dilute, the mean-square displacement is influenced both by direct interactions and hydrodynamic interactions. These interactions depend on the configuration of particles around the tracer. For hard spheres, the tracer will feel a change in configuration when it diffuses over a distance comparable to its radius. This sets the interaction time scale τ_I, which for hard spheres is a^2/D_0. On this time scale the mean-square displacement is in general no longer a linear function of time. The self-diffusion coefficient can still be defined through

$$\langle \Delta r^2(t) \rangle = 6D_s(t)t \ , \tag{3}$$

but is now a function of time. However, at times both short and long compared to τ_I the mean-square displacement is again linear in time. For short times $\tau_B \ll t \ll \tau_I$ the particle moves in a constant configuration of neighboring particles and is only influenced by hydrodynamic interactions which usually operate on a time scale comparable to τ_B. This defines the short-time self-diffusion coefficient $D_{s,S}$:

$$D_{s,S} = \frac{\langle \Delta r^2(t) \rangle}{6t} \ , \quad \tau_B \ll t \ll \tau_I \ . \tag{4}$$

For times $t \gg \tau_I$ the particle distorts the configuration of neighboring particles so that direct interactions as well as hydrodynamic interactions determine its mean-square displacement. This defines the long-time self-diffusion coefficient $D_{s,L}$:

$$D_{s,L} = \lim_{t \to \infty} \frac{\langle \Delta r^2(t) \rangle}{6t} \ . \tag{5}$$

In order to measure long-time diffusion in mixtures, the experimental time scale should be long enough to allow particles of each type to interact many times with particles of all other types. This means that the interaction time scale τ_I is set by the slowest particle. For the system used in this work this corresponds to $\tau_I = 0.1$ s. In a FRAP experiment the long-time limit is ensured by making the fringe spacing, which sets the length scale of the measurement, much larger than the size of the largest particle.

Theoretical calculations of the long-time self-diffusivity of multicomponent colloidal dispersions in the literature are scarce. There seem to be two approaches available at present. The first, due to Batchelor [14], calculates the friction that is felt by a tracer particle when it is slowly pulled through a multicomponent dispersion by means of a small external force. This theory is exact for hard spheres up to the pair interaction level, taking into account both hydrodynamic interactions and the extra friction due to the distortion of the pair distribution function. The second approach that we want to mention uses memory functions that are designed to give the exact short-time results, but which approximate the long-time behavior [11]. This theory is applicable to dilute but strongly interacting dispersions of highly charged spheres at low ionic strength. Because of the long range nature of the direct interactions in such systems the theory does not take hydrodynamic interactions into account.

Since the present work was done on hard-sphere dispersions, where hydrodynamic interactions play an important role, we shall compare our results with Batchelor's theory [14]. His results for the long-time self-diffusion coefficient can be written as

$$\frac{D_{s,L}^{(i)}}{D_0^{(i)}} = 1 + \sum_{k(\neq i)} K'_{ik}\phi_k \ , \tag{6}$$

valid up to first order in the volume fractions ϕ_k. Here the superscript (i) refers to a particle of type i. The coefficients K'_{ik} depend solely on the size ratio $\lambda = a_k/a_i$, and are always negative. They describe the reduction of the diffusivity of an i particle due to interactions with particles of type k. For the short-time limit the result is identical in form to Eq. (6) but with different values for the coefficients, which have been tested in Ref. [12]. Note that the summation in (6) excludes the term $k = i$. Equation (6) therefore describes tracer particles with a vanishing volume fraction. It can be made applicable to a two-component mixture by considering a three-component system with the tracer particle being identical to the second component but different from the third (say $k = j$). Thus

$$\frac{D_{s,L}^{(i)}}{D_0^{(i)}} = 1 + K'_{ii}(\lambda = 1)\phi_i + K'_{ij}(\lambda = a_j/a_i)\phi_j \ , \tag{7}$$

where the dependence on λ is denoted explicitly. The diffusion coefficient of a j particle is found by exchanging the indices i and j. For K'_{ii} Batchelor found the monodisperse value of -2.10. For the present size ratio of 9.3 the values of K'_{ij} and K'_{ji} can be found from his work by interpolating the numerical values in Ref. [14] to $\lambda = 9.3$

and 1/9.3, respectively. Substituting for the indices $i=S$ (small) and $j=L$ (large) the results are

$$\frac{D_{s,L}^{(S)}}{D_0^{(S)}}=1-2.10\phi_S-1.07\phi_L \ , \tag{8a}$$

$$\frac{D_{s,L}^{(L)}}{D_0^{(L)}}=1-2.10\phi_L-2.38\phi_S \ . \tag{8b}$$

For higher volume fractions three- and more-particle interactions become important, leading to correction terms of order ϕ^2 and higher. The corresponding coefficients are unknown and approximations for $D_{s,L}^{(i)}$ are known only for monodisperse spheres.

III. EXPERIMENTAL DETAILS

A. Preparation of the colloidal systems

Four types of colloidal particles were prepared: A fluorescently labeled particle FS and its nonfluorescent counterpart S, both having a radius of 39 nm, were used as the small particles. The large particles were the fluorescent FL and the nonfluorescent L particles, both of which had a radius of 365 nm. For the silica synthesis we followed the method described by Stöber, Fink, and Bohn [15]. The cores of the particles were labeled with the fluorescent dye fluorescein isothiocyanate (FITC) following the procedure of Van Blaaderen and Vrij [16]. A concise description of the synthesis is given in the following.

The particles were synthesized by adding freshly distilled tetraethoxysilane (TES, Fluka) to a mixture of distilled ethanol and ammonia (25%, Baker) under stirring. The initial amounts of reactants were chosen such as to obtain particles somewhat smaller than the desired final size. To obtain the fluorescent particles we added, in addition to the TES, a 1:10-mol/mol mixture of FITC and 3-(aminopropyl)triethoxysilane (APS, Janssen) that had been allowed to react for 24 h under stirring. The amount of FITC that was used corresponded to 1.7×10^3 and 9.4×10^5 molecules per particle for the FS and FL systems, respectively. After the silica particles had grown to completion (in one day) their size was determined using dynamic light scattering (for the small particles) or static light scattering (for the large particles). Then the particles were grown further by seeding the reaction mixture with extra TES in order to cover the dye molecules with a layer of pure silica. The relative amounts of the TES additions were chosen such that the resulting particles in corresponding systems (FS and S on the one hand, and FL and L on the other) would grow to nearly the same size. The sizes were measured again and were fine tuned in a last step by adding a small amount of TES in order to obtain exactly equally sized particles in the corresponding systems.

All four colloidal systems were transferred to a solution of 0.0100-M LiCl in dimethylformamide (DMF, Baker). For the large particles this was accomplished simply by repeated sedimentation under gravity and redispersion. The small particles, however, are sensitive to aggregation when centrifugated in ethanol at the high speeds that are required to sediment them. Therefore, the ethanol was gradually replaced with DMF by distillation under reduced pressure. Then an amount of 0.1-M LiCl solution in DMF was added to adjust the ionic strength approximately to 0.01 M. Finally, the dispersion was centrifugated once at 3000 rpm and redispersed in DMF (0.0100-M LiCl). A concentrated stock dispersion was prepared of each particle by sedimentation and removal of an amount of solvent. Other volume fractions were then prepared by diluting a weighted amount of stock dispersion with a weighted amount of DMF (0.0100-M LiCl).

B. Characterization of the dispersions

Results of the characterization of the four colloidal particles are collected in Table I. Static light scattering (SLS) was used to measure the size of the large particles in very dilute suspensions in ethanol at a wavelength of 546 nm. A 546-nm bandpass filter was used to eliminate the (small) fluorescent contribution to the scattered radiation. The measured scattering curves were fitted to theoretical curves calculated with the Mie scattering coefficients. From transmission electron micrographs the polydispersities σ, defined as the standard deviation in the radius divided by the mean radius, were determined from several hundreds of particles.

Dynamic light scattering (DLS) was done on dilute samples in DMF (0.01-M LiCl) at 25.0 °C using the 647.1-nm line from a Krypton laser (Spectra Physics model 2020), and at scattering angles ranging from 35° to 120°. These experimental diffusion coefficients are averages over many particles, where each particle contributes as $\sim$(radius)^6. In order to obtain an unweighted average, the value found can be corrected for the polydispersity in the way described in the Appendix. For the small particle systems this makes a significant difference: D_0 is a factor of 1.078 larger than the bare DLS result. *The DLS-data in Table I have been corrected in this way.* The par-

TABLE I. Results of particle characterization. DMF contains 0.0100-M LiCl.

Particle		L	FL	S	FS
a(SLS) (nm)		365±5	365±5		
a(DLS) (nm)	(DMF)	360±10	370±8	39±1	39±1
	(ethanol)			35±1	35±1
D_0 (10^{-12} m^2/s)	(DMF)		0.739±0.015	6.37±0.18	6.39±0.16
σ		0.03	0.03	0.12	0.12
particle density	(g/cm^3)	2.03±0.05	2.00	2.03	2.08

ticle radii were then calculated from this corrected D_0 using the Stokes-Einstein relation (2).

For completeness we mention that the fluorescent material is contained inside a core of radius 34 nm for the FS particles and 186 nm for the FL particles. The absorption and emission maxima are at about 500 and 540 nm, respectively. The refractive index of all the particles was 1.45, which is relatively close to that of DMF (1.43).

Also included in Table I are the DLS radii of particles FS and *S* dispersed in ethanol. These were found to be systematically 4 nm smaller compared to the DMF case. This very probably reflects the presence of a solvation layer which is considerably thicker in DMF, and gives rise to an increased hydrodynamic radius (see further Sec. III C).

Because of the presence of a solvation layer and because of the hydrodynamic nature of the measurements presented in this paper, we used a hydrodynamic volume fraction as a measure of concentration. Effective hydrodynamic volume fractions ϕ of the four stock dispersions were determined with the following procedure. First, a dry silica volume fraction ϕ_{sil} was determined from measurements of the dispersion density and the dry silica weight fraction. Weight fractions were found by drying a weighted amount of dispersion at 80 °C under nitrogen and reweighing, and were corrected for the small amount of LiCl present. This procedure also yields the dry particle density which is included in Table I. Then a series of dilutions was prepared in the low volume fraction range ($\phi_{\text{sil}}=0-0.02$). Their viscosities were measured using an Ubbelohde capillary viscometer (Schott-Geräte) thermostatted at 25.0 °C. The intrinsic viscosity

$$[\eta]=\lim_{\phi_{\text{sil}}\to 0}(\eta/\eta_0-1)/\phi_{\text{sil}} \tag{9}$$

was determined using quadratic regression. For uncharged spheres $[\eta]$ has the Einstein value of 2.5. The hydrodynamic volume fraction is then obtained as $\phi=([\eta]/2.5)\phi_{\text{sil}}$. For the large spheres the factor $[\eta]/2.5$ was about 1.2. For the small particles we found a larger value of 1.5, reflecting the relatively larger contribution of the solvation layer. All volume fractions ϕ reported in this paper are hydrodynamic volume fractions determined in this way. The relative error in the volume fractions is estimated to be 0.5%, or about 0.002 at $\phi=0.4$.

C. Particle interactions

In DMF the surfaces of the silica particles acquire a negative charge due to deprotonation of silanol groups. This surface charge is screened by a cloud of Li^+ and Cl^- ions in the solution. The thickness of this electrical double layer is characterized by the Debye screening length $1/\kappa$, with κ^2 given by

$$\kappa^2=\frac{2e^2cN_A}{\varepsilon kT}\ , \tag{10}$$

where c is the 1-1 electrolyte concentration, e the elementary charge, N_A Avogadro's number, ε the solvent permittivity, k Boltzmann's constant, and T the absolute temperature. At the present ionic strength (0.01 M), $1/\kappa$ has the value 2.2 nm, taking into account that the degree of dissociation of LiCl in DMF at 25 °C equals 0.88 [17]. This is small compared to the radii of both the small and large spheres, making their repulsions essentially hard sphere like. The particles will then behave as hard spheres, provided that the short ranged attractive van der Waals force is unimportant. This is the case for the present system due to the presence of a solvation layer around the particles. For silica in water it has been found, by means of surface force measurements, that the van der Waals force is effectively screened by a hydration layer of 3- or 4-nm thickness on each surface [18–20]. The hydration layer is probably formed by water molecules coordinated by surface silanol groups and adsorbed counterions [19,20], and it presents a steep force barrier located at a larger separation than the distance where van der Waals forces become active. From our finding of a 4-nm increase in the hydrodynamic radius of the small particles in going from ethanol to DMF and from their large hydrodynamic volume (Sec. III B), we conclude that DMF gives rise to a similar solvation layer. The absence of a significant van der Waals attraction also explains why the silica sols remain stable in DMF even at LiCl concentrations higher than 0.3 M. A solvation layer of 4 nm should even incorporate most of the double layer. Furthermore, van der Waals forces are not expected to be very strong due to the small difference in refractive index between particles and solvent (0.02). We conclude, therefore, that silica spheres in DMF (0.01-M LiCl) are good model hard-sphere systems.

D. Binary mixtures and their phase behavior

Binary mixtures with size ratio $a_L/a_S=9.3$ were prepared by mixing weighted amounts of the stock dispersions in a range of different proportions with either the small or large spheres being fluorescently labeled. Note that, in order to measure self-diffusion coefficients with FRAP, the fluorescent component need not necessarily be present only in trace amounts. A mixture of FL and *S* will be referred to as FLinS (fluorescent large spheres in a dispersion of small spheres). Analogously, FSinL stands for a mixture of FS and *L*. A wide range of compositions ϕ_L/ϕ_S was used. By subsequent dilutions of a mixture at a certain composition with the solvent, a straight line is traced toward the origin in the phase diagram. In this way the entire phase diagram was covered twice: once for FLinS and once for FSinL. In some cases mixtures were concentrated by centrifugation in order to reach regions higher up in the phase diagram. For the mixtures the uncertainties in the volume fractions are again estimated at $\Delta\phi_i/\phi_i=0.005$.

The mixtures were contained in tubes of relatively large diameter (5–10 mm), and their phase behavior was observed over one or two days. In addition, small amounts were transferred to glass vials of thickness 0.2 or 0.4 mm, width 4 mm, and length 100 mm (Vitro Dynamics) which were sealed at both ends to prevent evaporation of the solvent. These were monitored over a prolonged period of time and were also used for the FRAP

measurements (see Sec. III E). The large spheres sediment at a considerable rate (1 mm/h) in the more dilute samples. However, at larger volume fractions, say $\phi_L+\phi_S>0.3$, the rate of sedimentation is much smaller, and samples do not show significant sedimentation even after several days, allowing sufficient time for observation. This is due not only to an increase in solvent backflow but also, especially in samples rich in small spheres, to a decreased difference between the density of the large spheres and the effective density of the solvent containing the small spheres.

E. Fluorescence recovery after photobleaching

To determine long-time self-diffusion coefficients, fluorescence recovery after photobleaching (FRAP) was used [21–23]. In this technique a laser light interference fringe pattern is created in the dispersion by crossing two laser beams under an angle 2θ. The wave vector k of the fringes is

$$k=\frac{4\pi}{\lambda}\sin\theta \ , \tag{11}$$

where λ is the wavelength of the laser light. First, with a short and intense pulse, part of the FITC molecules is irreversibly destroyed (photobleached). This leaves a sinusoidal profile of unbleached molecules in the dispersion which fades away as a result of Brownian motion of the colloidal particles. All particles remain statistically identical since bleaching does not affect the way they interact. The decay of the bleached pattern is then monitored by oscillating the same fringes over the bleached pattern, but with a much lower intensity to avoid further bleaching. This is achieved by modulating the path length of one of the beams by means of a piezoelectric modulator with a typical frequency of 1 kHz. The measured fluorescent intensity then oscillates at the same frequency as the monitoring and bleached fringes fall into and out of phase, with the amplitude decreasing as the pattern fades. After electronic filtering at the modulation frequency, the resulting FRAP signal $S(t)$ is proportional to the long-time self-intermediate scattering function, and decays exponentially as

$$S(t)\propto\exp\{-D_{s,L}k^2t\} \ . \tag{12}$$

The proof that FRAP measures long-time self-diffusion in monodisperse systems, given in Ref. [23], can be straightforwardly carried over to binary systems. The small values of k used (2×10^5–8×10^5 m^{-1}) correspond to large wavelengths (8–30 μm), and ensure that the long-time limit is measured.

The setup that was used is described in Ref. [23], with the only modification that we used a photodiode as the detector instead of a photomultiplier tube. A Spectra Physics series 2000 argon laser provided the 488-nm light. The bleaching power was 200 mW, with bleach times ranging between 0.2 and 1 s depending on the sample. We verified that the bleach times did not influence the results. During the monitoring phase the intensity was reduced by a factor of 500–2000. The beam diameter was typically 2 mm. Samples were measured in the thin glass vials mentioned in Sec. III D. The measured signals were fitted to Eq. (12) including an additional constant to fit a small noisy background or a nondecaying component.

In each sample, 15–20 measurements were recorded at different positions in the cuvette. The results were averaged to obtain $D_{s,L}$ with a resulting statistical error of 3% for particles FS and 6% for FL. The larger error in the results of the large spheres is caused by the weaker fluorescent signal from these particles. Diffusion coefficients were normalized on D_0, the value at infinite dilution as measured with DLS (see Table I). Since ambient temperatures during the FRAP measurements were slightly below 25 °C (22–23°C), a small correction to D_0 was made through the solvent viscosity using Eq. (2). For the temperature dependence of the viscosity we found η_0(mPa s)$=0.822-0.010(T-25.0\,^\circ\text{C})$ using an Ubbelohde viscometer.

A final correction to the data was made to allow for the fact that DLS and FRAP measure different moments of the particle size distribution (the sixth and third, respectively). In the Appendix it is shown how the nth moment average can be related to a flat average depending on the polydispersity, Eq. (A7). For the small spheres with a polydispersity of 0.12 this leads to a small but noticeable difference. D_0 measured with DLS (Table I) was already corrected in this way, as discussed in Sec. III B. The $D_{s,L}$ values were corrected in the same way, using Eq. (A7) with $n=3$. This means that the bare values have been multiplied by a factor of 1.030. Using these corrections, the measured diffusion coefficients are seen to extrapolate nicely to $D_{s,L}/D_0=1$ at low volume fractions (see Sec. IV B). Note, however, that this procedure can only be applied at the level of D_0. As soon as particle interactions come into play the influence of polydispersity is a different matter, although recent Brownian dynamics simulations [24] showed that, at least for one-component hard-sphere dispersions, a not too large polydispersity has only a marginal influence on $D_{s,L}$.

IV. RESULTS AND DISCUSSION

We start this section with a description of the phase behavior and the determination of the phase diagram. The results of the long-time self-diffusion measurements are presented and discussed in Sec. IV B. Finally, measurements in the metastable region of the phase diagram are treated in Sec. IV C.

A. Phase behavior

In Fig. 1 the phase diagram of the binary mixture is shown. The nature of the different phases is indicated. The determination of the phase lines of this system has been described in Ref. [8]. In the largest part of the diagram the two components formed a fluid mixture (F) that remained homogeneous for many days after mixing. In the region indicated by $F+C$, mixtures phase separated into a colloidal fluid and a colloidal crystal formed by the large spheres. Some time after homogenization, crystals became visible in the bulk fluid due to Bragg reflections.

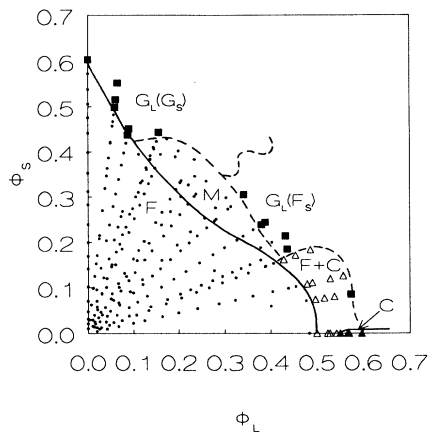

FIG. 1. Phase diagram of the binary hard-sphere mixture. Dots represents mixtures remaining homogeneous fluids, open triangles are samples separating into a fluid and a crystal, filled triangles are completely crystalline, and filled squares are glass states. The solid line indicates the fluid-solid binodal, and dashed lines are glass transition lines.

They nucleated homogeneously throughout the samples and then settled under gravity within a day or so, forming a crystalline sediment that was well separated from the fluid.

Although actual crystallization was observed only in a limited part of the phase diagram, it was possible to construct the fluid-solid binodal by a determination of the compositions of coexisting phases. This procedure has been described in Ref. [8], and the binodal found is represented by the solid line in Fig. 1. For the one-component system the volume fractions of freezing and melting ϕ_f and ϕ_m were found to be 0.497 ± 0.004 and 0.547 ± 0.004, respectively, as measured on both the large sphere systems L and FL. These values compare quite well with the well-known hard-sphere values of 0.494 and 0.545 [25]. This indicates that the hydrodynamic volume fraction used in this work (see Sec. III B) is also a good estimate of the thermodynamic volume fraction. In mixtures, tie lines [shown in Fig. 1(b) of Ref. [8]] connect a composition of a solid phase on the melting line ($\phi_{m,L}$, $\phi_{m,S}$) with the composition of the fluid phase on the freezing line ($\phi_{f,L}$, $\phi_{f,S}$) with which it is in equilibrium. The melting line was assumed to lie at almost zero $\phi_{m,S}$ because in the large sphere crystals there is very little space left open for the small spheres. This extreme segregation was nicely visible by eye in mixtures FSinL. Here the mixtures, being moderately yellow, separated into an almost white crystalline sediment and a fluid that was strongly colored yellow.

The shape of the $F+C$ coexistence region agrees qualitatively with that predicted by recent theories of the depletion effect [26,27]. However, as discussed in Ref. [8], the fluid-solid binodal is located at considerably higher ϕ_S than these theories predict.

The time needed for crystals to become visible depended strongly on the amount of small spheres present. Whereas in the one-component system this took no more than 15 min, the appearance of crystallites was delayed to almost two days in the mixture with $\phi_I/\phi_S=2.650$. In mixtures with larger amounts of small spheres, crystals did not become visible within the time span available for observation before significant sedimentation took place (at least four days). Such samples were examined under a polarization microscope for the possible presence of very small crystallites, but none were found. Since these mixtures are situated above the binodal, they must be metastable. In the region in the phase diagram that is indicated by an M, the systems behaved like fluids, and complete relaxation of the FRAP signal of both components was observed.

At the highest concentrations samples became very viscous, and remained amorphous. These appeared to be glass states, since an arrest of the long-time self-diffusion of the large spheres was observed [28]. This was evidenced by an incomplete decay of the FRAP signal, indicating that the bleached pattern does not fade away in a finite time. Furthermore, the speckles in the scattering pattern of the large spheres were static, implying that these particles are dynamically arrested. An example of a FRAP measurement is shown in Fig. 2(a). Notice that the time scale of the experiment is extremely long. In Fig. 1 glass states are separated from homogeneous fluid phases by glass transition lines indicated by the dashed lines. When the long-time self-diffusion of the small spheres was measured, a marked difference in dynamical

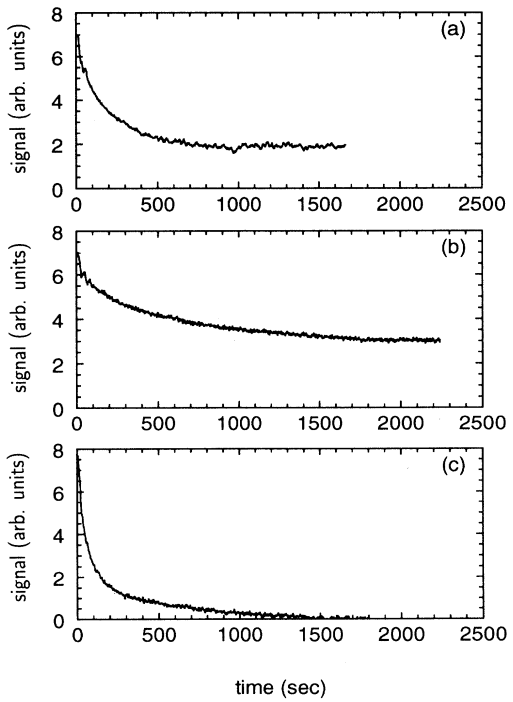

FIG. 2. Correlation functions of glassy samples measured with FRAP. (a) Large spheres measured at $k=463\,320\ \mathrm{m}^{-1}$ in a mixture of $\phi_L=0.0592$ and $\phi_S=0.499$ in the $G_L(G_S)$ state. (b) Small spheres measured at $k=206\,060\ \mathrm{m}^{-1}$ in a mixture of $\phi_L=0.0609$ and $\phi_S=0.516$ in the $G_L(G_S)$ state. (c) Small spheres measured at $k=203\,700\ \mathrm{m}^{-1}$ in a mixture of $\phi_L=0.379$ and $\phi_S=0.239$ in the $G_L(F_S)$ state.

behavior was found between glasses formed in systems that are rich in small spheres and those that are rich in large spheres. In the former case, the FRAP signals of the small spheres did not decay to zero [Fig. 2(b)], indicating glasslike behavior just like the large spheres. This glass state is therefore indicated by $G_L(G_S)$. In the latter case, however, the FRAP signals of the small spheres always showed complete relaxation [Fig. 2(c)], whereas in this region FRAP signals of large spheres always approached a nonzero value. Also, the scattering speckles were static. This implies that the small particles still behave like a fluid when the large ones are already glasslike. Therefore, this glass state is indicated by $G_L(F_S)$. We do not know the exact location of the boundary between the $G_L(G_S)$ and $G_L(F_S)$ states in Fig. 1, nor is it clear that there even exists a sharp boundary between the two glass states. The dynamics of the glass states will be analyzed more closely in Sec. IV C.

B. Long-time self-diffusion

In this section we adopt the following notation: In the symbol $D_{s,L}^{(i)}$ the *subscripts* s and L indicate the type of diffusion coefficient (long-time self). In mixtures, the *superscript* placed between parentheses refers to the type of particle (small or large) of which the diffusion coefficient is given. If no superscript appears, then a one-component system is implied.

In Fig. 3, $D_{s,L}/D_0$ is plotted versus the volume fraction in monodisperse suspensions containing either the small particles FS or the large particles FL. Despite the large difference in size the two sets of data coincide well, as expected for hard spheres. The data also agree well with earlier experimental results on hard-sphere dispersions [22,29]. In addition to the data in the literature, we have been able to measure $D_{s,L}$ of the small spheres to quite low volume fractions, thanks to the high fluorescence yield of these particles. This allowed us to give a reliable estimate of the low volume fraction behavior:

$$\frac{D_{s,L}}{D_0}=1-(2.02\pm0.10)\phi\ . \tag{13}$$

The first order in volume fraction coefficient, which describes the reduction of $D_{s,L}$ due to pair interactions, agrees well with the theoretical value of -2.10 [14,30]. For the large spheres, which gave a smaller fluorescent signal, we find the same value although with a larger uncertainty: -2.0 ± 0.2. At high volume fractions $D_{s,L}$ becomes very small, until at $\phi=0.604$ the measured FRAP signal did not decay to zero even over a very long-time span, so that $D_{s,L}=0$. This implies that somewhere between volume fractions 0.573 and 0.604 a point is reached where the correlation function takes an infinite time to relax. This is the glass transition volume fraction, which for hard spheres is close to 0.58 [31].

For binary mixtures that remained homogeneous, the long-time self-diffusion coefficients of the small spheres in the presence of large spheres (FSinL) are plotted in Fig. 4(a), and for the large spheres in the presence of small spheres (FLinS) in Fig. 4(b). The data of the one-component dispersions are included for comparison. The diffusivities are plotted versus the volume fraction of the labeled species, for several ratios ϕ_L/ϕ_S. It should be noted that, since the data were measured as series of dilutions at a constant ϕ_L/ϕ_S, the volume fraction of the unlabeled particles increases in constant proportion to the volume fraction of the labeled particles. All curves extrapolate to $D_{s,L}^{(i)}/D_0^{(i)}=1$ at low volume fractions, as they should. $D_{s,L}^{(i)}$ decreases monotonously with volume fraction, and more quickly so as the amount of unlabeled particles is increased. All curves are linear for volume fractions where $D_{s,L}^{(i)}/D_0^{(i)}>0.7$. It is surprising that linearity is found up to relatively high volume fractions, where a linear approximation in expansions such as those in Eq. (8) is not expected to be valid anymore.

From the linear initial slope the first order in volume fraction coefficient A can be obtained, which is defined as

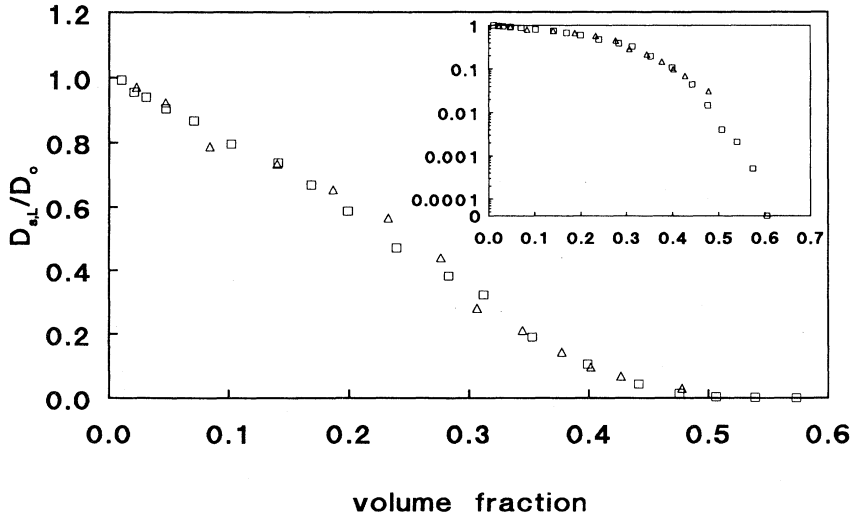

FIG. 3. Long-time self-diffusion coefficient vs volume fraction for the one-component dispersions FL (radius 365 nm, triangles) and FS (radius 39 nm, squares). Inset shows the same data on a semilogarithmic scale.

$$\frac{D_{s,L}^{(i)}}{D_0^{(i)}}=1+A^{(i)}\phi_i \ , \quad i=S,L \ . \tag{14}$$

In terms of Batchelor's theory, Eq. (8), the quantities $A^{(S)}$ and $A^{(L)}$ should depend linearly on the ratios ϕ_L/ϕ_S and ϕ_S/ϕ_L, respectively:

$$A^{(i)}=K'_{ii}+K'_{ij}\frac{\phi_j}{\phi_i} \ . \tag{15}$$

In Fig. 5 the data and theoretical lines have been plotted in this way. The first order behavior of the small spheres follows the theory very well. A weighted least squares fit to the data yields

$$\frac{D_{s,L}^{(S)}}{D_0^{(S)}}=1-\left[(1.97\pm0.08)+(1.10\pm0.08)\frac{\phi_L}{\phi_S}\right]\phi_S \ , \tag{16}$$

which should be compared to the theoretical result in Eq. (8a). For the large spheres we also find the linear behavior of $A^{(L)}$:

$$\frac{D_{s,L}^{(L)}}{D_0^{(L)}}=1-\left[(1.96\pm0.13)+(1.14\pm0.09)\frac{\phi_S}{\phi_L}\right]\phi_L \ . \tag{17}$$

Comparison with the theoretical result, Eq. (8b), shows that the intercept, which is determined by L-L interactions, has the expected value. However, the slope, determined by L-S interactions, is a factor of 2 smaller than the theory predicts, resulting in a diffusion coefficient that is somewhat larger than expected.

The lack of agreement for the large sphere's diffusion coefficients probably has its origin in the experimental circumstance that there is a huge difference between the numbers of large and small particles. This is a consequence of the extreme difference in the volumes of the two species: for all practical values of ϕ_L/ϕ_S the number of small spheres exceeds the number of large spheres by a factor of more than 100. As a result, even in a dispersion as dilute as $\phi_L+\phi_S=0.01$, a large sphere is very unlikely to interact with only one small particle at a time. For

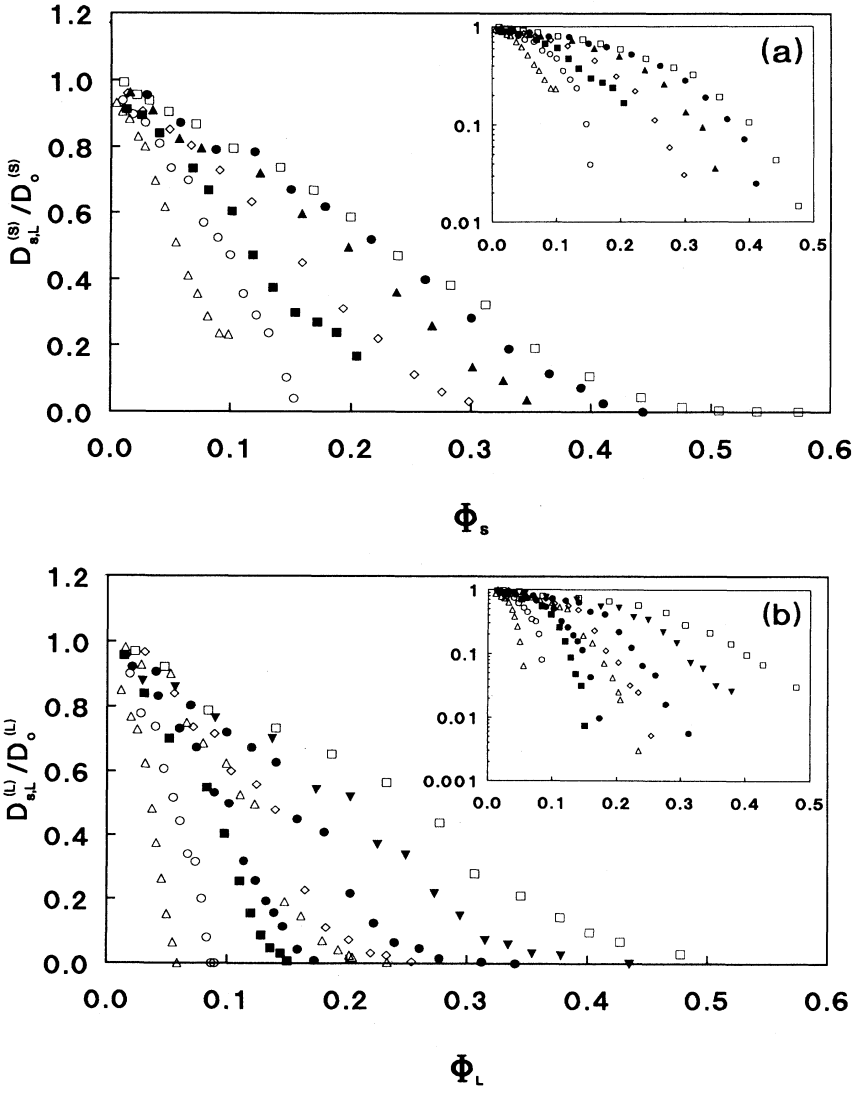

FIG. 4. (a) Long-time self-diffusion coefficients of the small spheres in mixtures of compositions (from left to right curve) $\phi_L/\phi_S=4.424$, 2.650, 1.588, 1.012, 0.677, 0.349, and pure hard spheres. (b) Long-time self-diffusion coefficients of the large spheres in mixtures of compositions (from left to right curve) $\phi_L/\phi_S=0.119$, 0.199, 0.356, 0.403, 0.610, 0.775, 1.121, 2.357, and pure hard spheres. Insets show the same data on a semilogarithmic scale.

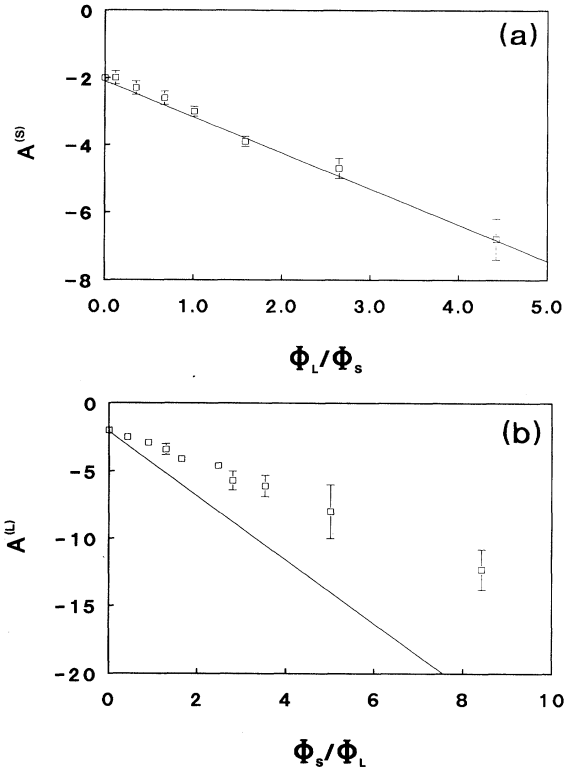

FIG. 5. First order in volume fraction coefficients of $D_{s,L}^{(i)}$ as defined in Eq. (14). (a) Data for small spheres versus ϕ_L/ϕ_S. (b) Data for large spheres versus ϕ_S/ϕ_L. Lines are the theoretical results from Ref. [14] given in Eq. (8).

this reason the theoretical value $K'_{LS}=-2.38$, in which only pair interactions have been taken into account, is probably not applicable. It seems more likely, therefore, that the measured value $K'_{LS}=-1.14$ corresponds to the friction of a large sphere moving through a dispersion of small spheres which is in itself dilute in the sense that the small spheres undergo almost exclusively two-particle interactions.

It is difficult to estimate how this should influence $D_{s,L}^{(L)}$. A theoretical prediction for the present experiment should include the distortion of the pair distribution function for the correlations between the small and large spheres, as a large sphere is pulled through the dispersion, and interacts with *many* small spheres simultaneously, not just a single one. Such a theory is not yet available.

One effect that is due to interactions of large spheres with many small spheres simultaneously is an effective attraction between the large spheres. This depletion attraction [6,7] does not provide an explanation for the larger diffusion coefficient found experimentally, however. Several theoretical approaches have incorporated the effect of interparticle interactions on $D_{s,L}$ (in addition to the hard-core repulsion) up to the pair level [14,32,33]. Venkatesan, Hirtzel, and Rajagopalan [32] showed that, without hydrodynamic interactions, the first order in ϕ coefficient can become significantly less negative than -2. However, including hydrodynamics results in a value more negative. Cichocki and Felderhof [33], who gave the most accurate treatment, modeled interactions by a square well or step potential. They showed that in almost all cases an attraction decreases $D_{s,L}$ relative to the hard-sphere case. Only if the relative width of the well is not too small (>1.041) and if, at the same time, the attraction is very weak there is a slight increase. Both conditions are fulfilled in some of our low volume fraction experiments, but the predicted increase is far too small to explain our result.

In a binary mixture with given concentrations, it would of course be desirable to know the diffusion coefficients of both particle types. Such information can be extracted from Fig. 4 by comparing data on a mixture in which the small spheres are labeled, with another mixture with approximately the same ϕ_L/ϕ_S, in which the large spheres are labeled. Our data contain four of such complementary data sets. They are plotted in Figs. 6(a)–6(d) as $D_{s,L}^{(i)}/D_0^{(i)}$ versus the total volume fraction. These graphs enable one to compare the reduction of the mobility of the large spheres (triangles) with that of the small spheres (squares) with increasing volume fraction, in a dispersion with a fixed composition. In a dispersion with a small proportion of large spheres [$\phi_L/\phi_S=0.118$, Fig. 6(a)] it is seen that the diffusion coefficient of the small spheres (relative to D_0) is generally smaller than that of the large spheres. This difference increases to about 50% at high concentrations. Evidently, the presence of the many small spheres obstructs the motion of a small sphere more than it obstructs the motion of a large sphere. At a somewhat larger proportion of large spheres [$\phi_L/\phi_S=0.35$, Fig. 6(b)] the reduction of the mobility is just about the same for both spheres over the entire range of volume fractions. For $\phi_L/\phi_S\approx 1.1$ in Fig. 6(c) we see that, at higher concentrations, the relative diffusion coefficient of the large spheres has decreased and is now smaller than that of the small spheres. Finally, at $\phi_L/\phi_S=2.5$ [Fig. 6(d)], the mobility of the small spheres has considerably increased and is now well above that of the large spheres. Hence the exchange of a number of small spheres for a few large spheres, having the same total volume, increases the mobility of the remaining small spheres and decreases the mobility of the large spheres. The increase in the mobility of a small sphere is the result of a large increase in the *free volume* available to a small sphere. This is because 800 small spheres have a much larger excluded volume than a single large sphere, although the total particle volume is the same. The fact that at the same time the mobility of the large spheres decreases means that their mobility is hindered more strongly by the obstructing effect of the other large spheres than by the friction caused by the small ones.

As mentioned above, a tracer particle, whether it is small or large, interacts much more frequently with small particles than with large ones, since the former are much more abundant and much more mobile (they have a larger D_0). Between collisions with large particles the tracer effectively diffuses through a dispersion containing only small particles. Therefore, a small tracer particle is interacting most of the time with a neighbor cage of other small particles, while the large particles are obstacles

which it has to diffuse around. A large tracer particle, on the other hand, is so large that is can only be encaged by other large spheres, while the small spheres merely slow down its motion inside the cage. In this view, the interactions between the tracer and small spheres become decoupled from the interactions between the tracer and large spheres as a result of the large difference in time and length scales. These considerations led us to a model to describe the $D_{s,L}^{(i)}$ data in a way that is somewhat similar in spirit to an idea of Medina-Noyola [34]. He suggested to separate $D_{s,L}$ for a one-component system into a factor $D_{s,S}$, accounting for the hydrodynamic interactions that operate on a short-time scale, and a factor accounting for collisions between particles, that take place on a much longer time scale. First, imagine a single small tracer particle placed in a dispersion containing only large spheres, and suppose we know its diffusion coefficient $D_{s,L}^{(S)}(\phi_S \to 0, \phi_L)$. Then add many other small spheres up to an overall volume fraction of ϕ_S. Between interactions with the large spheres, the tracer now diffuses through a dispersion of other small spheres with an effective volume fraction of about $\phi_S/(1-\phi_L)$ due to the excluded volume of the large spheres. Motion through the dispersion of small spheres reduces the tracer's diffusion coefficient by a factor of $D_{s,L}[\phi_S/(1-\phi_L)]/D_0$, which is just the one-component hard-sphere value. The resulting diffusion coefficient is then

$$D_{s,L}^{(S)}(\phi_S,\phi_L)=D_{s,L}^{(S)}(\phi_S\to 0,\phi_L)\frac{D_{s,L}\left[\dfrac{\phi_S}{1-\phi_L}\right]}{D_0} . \quad (18)$$

If, on the other hand, the tracer is a large sphere, then its diffusion coefficient, when placed in a dispersion of other large spheres, is given by the one-component value $D_{s,L}^{(L)}(\phi_L)$. Again, small spheres are added. Between collisions with the large spheres the tracer is slowed down by a factor of $D_{s,L}^{(L)}[\phi_S/(1-\phi_L),\phi_L\to 0]/D_0^{(L)}$ which is the (relative) diffusion coefficient of a single large sphere in a dispersion of small spheres. Hence

$$D_{s,L}^{(L)}(\phi_S,\phi_L)=D_{s,L}^{(L)}\left[\frac{\phi_S}{1-\phi_L}\ ,\ \phi_L\to 0\right]\frac{D_{s,L}(\phi_L)}{D_0} . \quad (19)$$

Equations (18) and (19) can be used to predict $D_{s,L}^{(i)}$ in a mixture of any composition, starting from two limiting cases. The second factor on the right-hand sides of Eqs. (18) and (19) is the one-component quantity, which can be taken from Fig. 3. The first factor in either equation cannot strictly be measured, but can be estimated from the mixture with the smallest proportion of small, respectively large spheres. $D_{s,L}^{(S)}(\phi_S\to 0,\phi_L)$ can thus be obtained from the data on FSinL at $\phi_L/\phi_S=4.424$, divided by the second factor in (18) which is close to unity for this com-

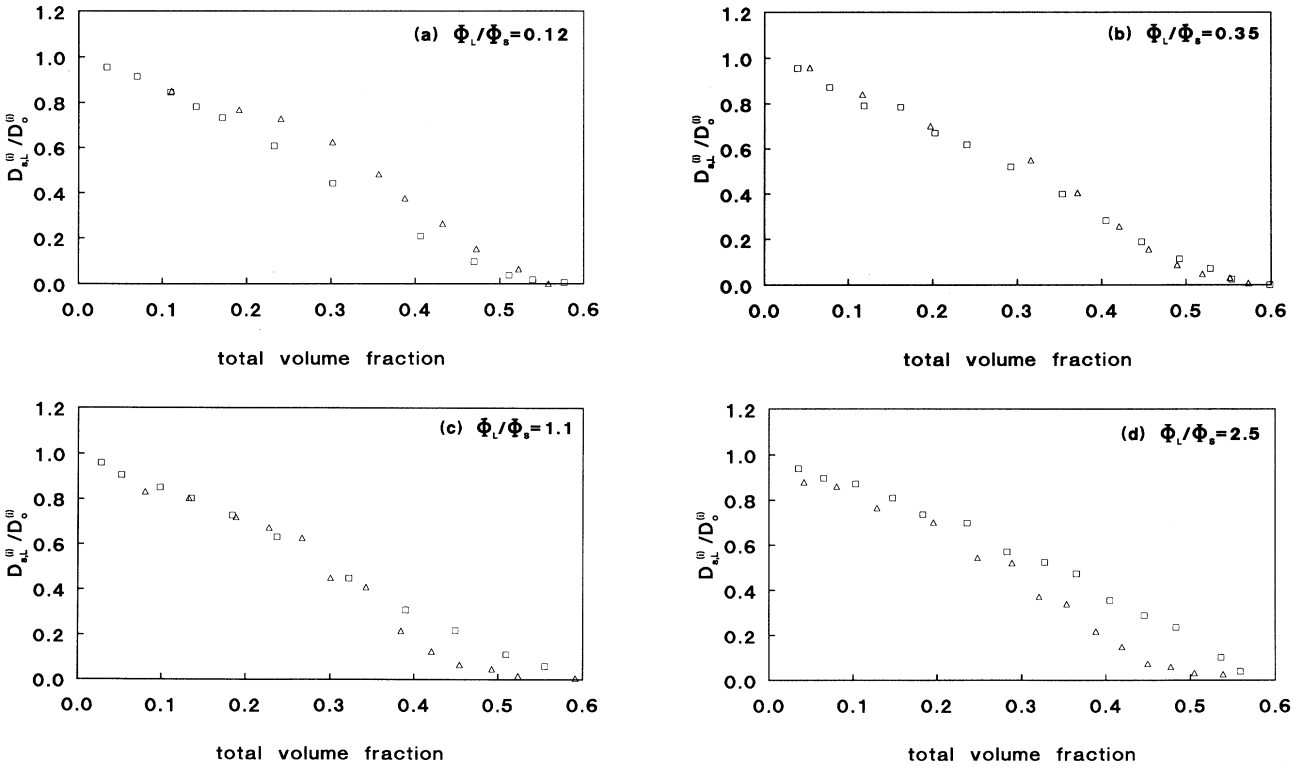

FIG. 6. $D_{s,L}$ of the small spheres (squares) and large spheres (triangles) vs the total volume fraction, measured in mixtures of almost equal composition. (a) $\phi_L/\phi_S=0.118$ for the mixture with small spheres labeled, and $\phi_L/\phi_S=0.119$ with the large spheres labeled. In the same order: (b) $\phi_L/\phi_S=0.349$ and 0.356, (c) $\phi_L/\phi_S=1.012$ and 1.122, and (d) $\phi_L/\phi_S=2.650$ and 2.357.

position, and is shown in Fig. 7(a). The factor $D_{s,L}^{(L)}[\phi_S/(1-\phi_L),\phi_L \to 0]$ follows from the data on FLinS at $\phi_L/\phi_S = 0.119$, divided by the second factor in (19), which is again almost 1, and is plotted in Fig. 7(b).

The predictions of Eqs. (18) and (19) at finite ϕ_L/ϕ_S are shown in Figs. 8(a) and 8(b) for several ϕ_L/ϕ_S together with the corresponding experimental points. It is seen that the small spheres' diffusion coefficient is predicted accurately up to high volume fractions. For large spheres, Eq. (19) follows the data well for mixtures with $\phi_L/\phi_S < 0.5$, including the downward curvature. However, for mixtures with a larger proportion of small spheres, $D_{s,L}^{(L)}$ is overestimated considerably at higher volume fractions. Since the physical picture that led to Eqs. (18) and (19) regards the interactions of a tracer with both types of particles as decoupled, the extra friction on the large spheres must be due to coupled interactions.

The model that we used to interpret particle mobilities and led to Eqs. (18) and (19) is admittedly too simple in that it ignores many-body hydrodynamics and some multiparticle interactions. Also, it applies only to mixtures of particles with a large difference in size. Nevertheless, it performs rather well, and provides a grip on a complicated problem for which no theories yet exist.

Combining theory and simulation, Kim and Torquato [35] obtained some results for the diffusion coefficient of a small but finite-sized tracer sphere in a porous medium modeled by a packing of hard spheres. Their results for a size ratio of 9 (from their Fig. 4) are included in Fig. 7(a) (indicated by +), and are seen to follow our data closely. Since their approach did not incorporate hydrodynamic interactions, and treated the large spheres as stationary instead of diffusive, the agreement might partly be the result of a cancellation of errors, but it could also mean that these effects have only a small influence on $D_{s,L}^{(S)}$. Experiments on small spheres diffusing through a crystal of (unlabeled) large spheres always resulted in a double exponential decay of the FRAP signal, one of the modes being very slow. Because of the polycrystalline nature of the dispersion it was not possible to separate the contributions from particles diffusing along grain boundaries, and those diffusing through the crystal.

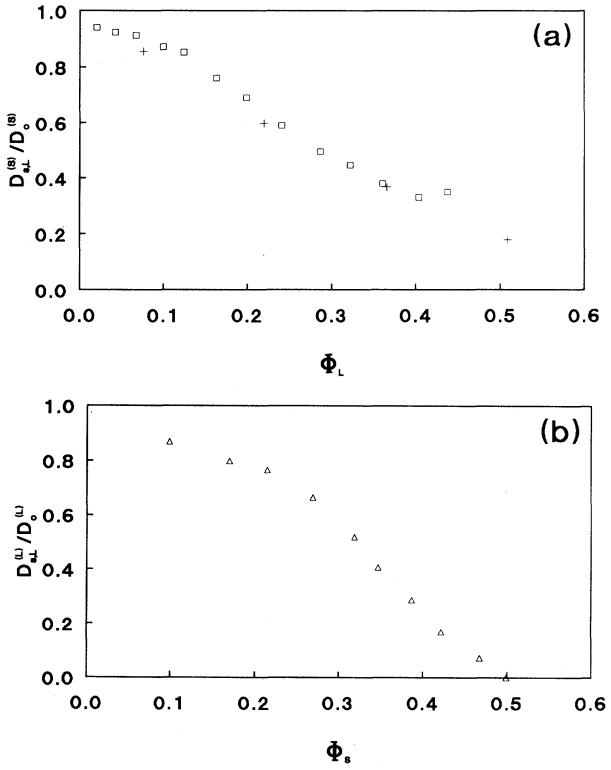

FIG. 7. (a) Data representing $D_{s,L}$ of a single small sphere in a dispersion of large spheres (squares), and predictions from Ref. [35] for a single sphere in a porous medium of large spheres with size ratio 9 (+). (b) Data representing $D_{s,L}$ of a single large sphere in a dispersion of small spheres. See text for details.

C. Mobility in metastable states

In Sec. IV A a distinction was made between three regions in the phase diagram that are situated above the fluid-solid binodal. Being in the two-phase region, all three are metastable states. In this section we will more closely consider the dynamics in these states.

Both of the glass states showed structural arrest, and this is the reason that they are unable to reach their true equilibrium states. In the metastable fluid state (M in Fig. 1), however, both particles in the mixture had a correlation function that always decayed monoexponen-

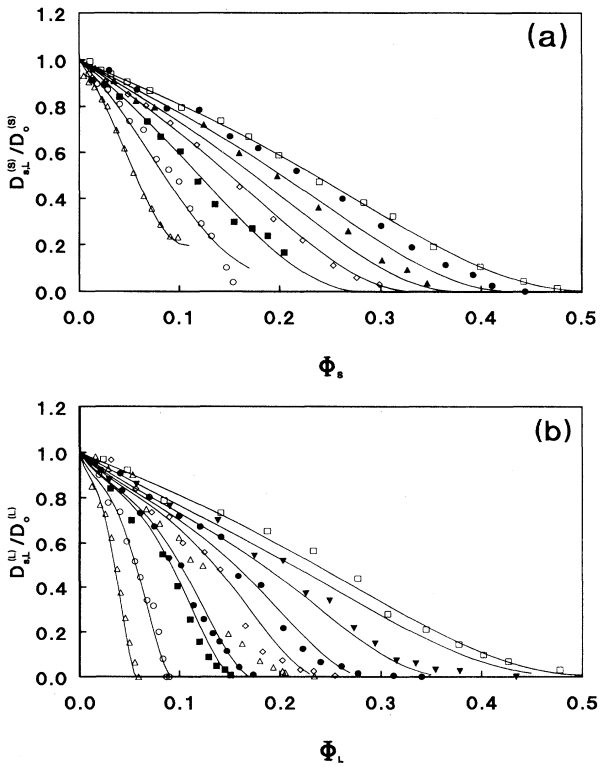

FIG. 8. Comparison between the measured $D_{s,L}$ (the points are the same as in Fig. 4) and predictions (solid lines). (a) Small spheres, Eq. (18); (b) large spheres, Eq. (19).

tially to zero. We cannot provide the complete explanation of why these mixtures failed to crystallize. It is conceivable that the rate of crystallization in mixtures with a small proportion of large spheres is very small, since it requires a considerable structural reordering. The formation of a crystal would require bringing together large particles from over large distances, and the simultaneous removal of many small particles from the interstices, making nucleation an unlikely event. The process would be slowed down even further by the very slow diffusion of the large spheres. From Fig. 4 it can be seen that $D_{s,L}^{(L)}$ for systems in the metastable region is more than a factor of 50 smaller than its value at infinite dilution. For a similar size ratio, crystallization was observed in Ref. [5] at very low ϕ_L, but only on the walls of the container, and at a much smaller ϕ_S.

The most apparent difference in dynamic behavior between the two glass states was already mentioned in Sec. IV A: although the large spheres are arrested in both states, the small spheres are arrested only in the $G_L(G_S)$ state, but still mobile in $G_L(F_S)$. A more detailed analysis revealed other differences. In both states the correlation function of the small spheres appears to have a fast relaxational mode and a much slower one (Fig. 2). For the $G_L(F_S)$ systems the two modes already appeared in samples slightly below the glass transition line, where the large spheres were still fluidlike (judged from the fluctuating speckles). All these FRAP signals could be fitted well to double-exponential curves. In order to compare the rates of relaxation with those in the fluid phase and with each other, a diffusion coefficient was assigned to each mode. The nonzero diffusion coefficients thus obtained are plotted in Fig. 9 vs ϕ_S for two mixtures, each in or near one of the two glassy states, together with those measured in the fluid region of the phase diagram. A clear difference between the two glass states is immediately seen. As a mixture is compressed into a $G_L(G_S)$ glass (squares), it develops a relaxational mode that is faster than in the fluid just below the glass transition.

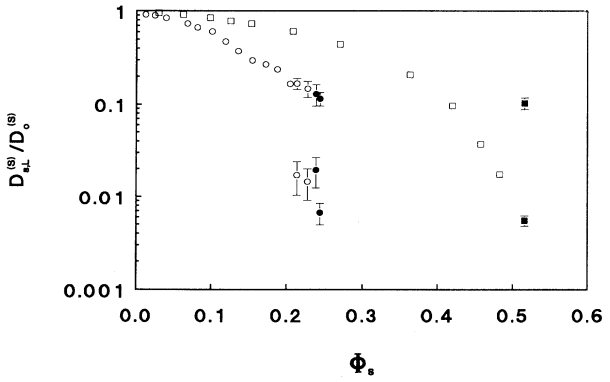

FIG. 9. $D_{s,L}^{(S)}$ vs ϕ_S on compressing a mixture into the $G_L(F_S)$ state ($\phi_L/\phi_S=1.588$, circles) and on compressing a mixture into the $G_L(G_S)$ state ($\phi_L/\phi_S=0.118$, squares). In points with error bars the relaxation was double exponential, and a diffusion coefficient was assigned to each mode. Solid symbols are glasses, open symbols fluids.

The same was seen in the one-component small sphere glass. The $G_L(F_S)$ state (circles), on the other hand, appears to develop a slower mode when the glass transition line is approached. Notice also that the diffusion coefficient of the small spheres just below the $G_L(F_S)$ glass transition is at least an order of magnitude larger than just below the $G_L(G_S)$ transition.

The appearance of a slower mode in the $G_L(F_S)$ state must be associated with the slowing down of the large spheres starting to form a glasslike structure. Evidently, both particle types need not always form a glass (i.e., become structurally arrested) simultaneously. As soon as the small spheres form a glass, the large ones will obviously become arrested as well, since they are completely embedded by them. This should happen in mixtures with a high volume ratio of small spheres, like in $G_L(G_S)$. However, the reverse is not true: when the large spheres have formed a static network, the cavities that are left open in the structure can still be wide enough to accommodate the motion of small particles. The two modes seen in Fig. 2(c) can then be explained by a relatively fast intracavity motion and a much slower diffusion from one cavity to another. As suggested by Fig. 9, both modes become slower as the glass is compressed. The origin of the partial decay of the FRAP signal for the small spheres in the $G_L(G_S)$ state is not clear.

Our diffusion measurements for the two glass states are rather preliminary so far. Clearly, a more detailed investigation, for example taking smaller steps in the volume fraction and by doing simultaneous DLS measurements on the large spheres, is needed for a better understanding.

V. CONCLUSIONS

We studied the phase diagram of, and long-time self-diffusion in, a binary colloidal dispersion with a size ratio of 1:9.3. This mixture shows a phase separation into a colloidal fluid and a colloidal large sphere crystal. Furthermore, an extended, long-lived metastable fluid region and two different glassy states are found [8]. The long-time self-diffusion coefficient of both particle species was extensively studied as a function of composition and total volume fraction. The first order in volume fraction coefficient of the one-component dispersions was found to be -2.0 ± 0.1. The low volume fraction behavior of the diffusivity of the small spheres in mixtures with large spheres was also completely in line with Batchelor's low volume fraction theory [14]. The experimental result is given in Eq. (16). The diffusion coefficient of the large spheres in mixtures with small spheres, Eq. (17), could not be explained by the theory. Due to the large difference in size between the particles, however, pair interactions between a large sphere and the many small spheres are expected to be very rare, so that the theory does not strictly apply. Theories incorporating many-particle interactions are not yet available for comparison with the data. For higher volume fractions, Eqs. (18) and (19) were therefore proposed, in which the friction experienced by a tracer particle due to the presence of the small spheres becomes effectively decoupled from the friction due to the large spheres. These formulas represent the

diffusivities reasonably well for the large spheres, and quite accurately for the small spheres.

The glassy states were identified by an incomplete decay of the correlation functions measured with FRAP. One type of glass state occurs in mixtures that are rich in small spheres. Here the small spheres form a glass that embeds the large spheres and arrests their motion as well. The other type of glass state, occurring in systems that are rich in large spheres, is unusual. Although the large spheres were structurally arrested, the small spheres still show a complete relaxation of the FRAP correlation function. Evidently, the small spheres are able to move through the cavities in the relatively open structure that is formed by the large spheres.

ACKNOWLEDGMENTS

We are grateful to G. Harder and M. van Amerongen for their technical assistance. We also thank C. Bouman and C. van der Werf for software development and implementation. This work is part of the research program of the Foundation for Fundamental Research on Matter (FOM) with financial support from the Netherlands Organization for Scientific Research (NWO).

APPENDIX

Here we calculate how the measured diffusion coefficient (in the limit of infinite dilution) is affected by the way in which a measuring technique weighs the contribution of a particle with radius a to the signal. DLS weighs a particle with its volume squared ($\sim a^6$) and therefore measures the sixth moment of the size distribution $P(a)$. FRAP weighs a particle with the number of dye molecules it carries. It therefore measures either the second or third moment of $P(a)$, depending on whether a thin shell ($\sim a^2$) or the core ($\sim a^3$) of the particle is labeled, respectively. We can write the measured correlation function $f^{\rm pol}$ of a dilute polydisperse suspension as

$$f^{\rm pol}(k,t)=\frac{\int da\, P(a)b(k,a)\exp\{-D_0(a)k^2t\}}{\int da\, P(a)b(k,a)}\ , \tag{A1}$$

where $b(k,a)$ describes the contribution to the signal of a particle of size a. The weight function b may also depend on the scattered wave vector k; for example, in DLS it also incorporates the form factor. We assume that $P(a)$ is sharply peaked, so that, writing

$$\exp\{-D_0(a)k^2t\}=\exp\{-D_0^{\rm pol}(k)k^2t\}\times\exp\{-[D_0(a)-D_0^{\rm pol}(k)]k^2t\}\ ,$$

we can expand the second exponent in powers of $D_0(a)-D_0^{\rm pol}(k)$ up to second order. After reexponentiation, we then obtain

$$f^{\rm pol}(k,t)=\exp\{-D_0^{\rm pol}(k)k^2t+\tfrac{1}{2}\sigma_D^2k^4t^2\}\ , \tag{A2}$$

with

$$D_0^{\rm pol}(k)=\frac{\int da\, P(a)b(k,a)D_0(a)}{\int da\, P(a)b(k,a)}\ , \tag{A3}$$

$$\sigma_D^2=\frac{\int da\, P(a)b(k,a)[D_0(a)-D_0^{\rm pol}(k)]^2}{\int da\, P(a)b(k,a)}\ . \tag{A4}$$

$D_0^{\rm pol}(k)$ is the polydisperse diffusion coefficient that is measured. In expression (A3) we now expand $b(k,a)D_0(a)$ around the average radius $\bar a$ up to second order in $a-\bar a$. The result is

$$D_0^{\rm pol}(k)=D_0(\bar a)+\frac{\sigma^2\bar a^2}{2b(k,\bar a)}\left[\frac{\partial^2}{\partial\bar a^2}(b(k,\bar a)D_0(\bar a))-D_0(\bar a)\frac{\partial^2}{\partial\bar a^2}b(k,\bar a)\right]\ , \tag{A5}$$

with the polydispersity σ defined by

$$\sigma^2=\frac{1}{\bar a^2}\int da\, P(a)(a-\bar a)^2\ . \tag{A6}$$

Now we use that $D_0(a)\sim 1/a$ and $b(k\to 0,a)\sim a^n$ with $n=2$, 3, and 6, depending on the measuring technique, and find

$$D_0^{\rm pol}(k\to 0)=D_0(\bar a)[1-(n-1)\sigma^2]\ . \tag{A7}$$

This equation is used in Secs. III B and III E to obtain $D_0(\bar a)$ from DLS and FRAP measurements.

[1] S. Hachisu and S. Yoshimura, Nature **283**, 188 (1980).
[2] P. Bartlett, R. H. Ottewill, and P. N. Pusey, J. Chem. Phys. **93**, 1299 (1990); Phys. Rev. Lett. **68**, 3801 (1992).
[3] S. Sanyal, N. Easwar, S. Ramaswamy, and A. K. Sood, Europhys. Lett. **18**, 107 (1992).
[4] J. S. van Duijneveldt, A. W. Heinen, and H. N. W. Lekkerkerker, Europhys. Lett. **21**, 369 (1993).
[5] P. D. Kaplan, J. L. Rouke, A. G. Yodh, and D. J. Pine, Phys. Rev. Lett. **72**, 582 (1994).
[6] S. Asakura and F. Oosawa, J. Polym. Sci. **32**, 183 (1958).
[7] A. Vrij, Pure Appl. Chem. **48**, 471 (1976).
[8] A. Imhof and J. K. G. Dhont, Phys. Rev. Lett. **75**, 1662 (1995).
[9] G. D. J. Phillies, J. Chem. Phys. **81**, 1487 (1984).
[10] R. Krause, G. Nägele, J. L. Auraz-Lara, and R. Weber, J. Colloid Interface Sci. **148**, 231 (1992).
[11] G. Nägele, T. Zwick, R. Krause, and R. Klein, J. Colloid Interface Sci. **161**, 347 (1993).
[12] P. D. Kaplan, A. G. Yodh, and D. J. Pine, Phys. Rev. Lett. **68**, 393 (1992).
[13] X. Qiu, D. Ou-Yang, and P. M. Chaikin, J. Phys. (Paris) **49**, 1043 (1988).
[14] G. K. Batchelor, J. Fluid Mech. **131**, 155 (1983); **137**, 467 (1983).
[15] W. Stöber, A. Fink, and E. Bohn, J. Colloid Interface Sci. **26**, 62 (1968).
[16] A. van Blaaderen and A. Vrij, Langmuir **8**, 2921 (1992).
[17] J. Prue and P. J. Sherrington, Trans. Faraday Soc. **57**,

1795 (1961).
[18] G. Peschel, P. Belouschek, M. M. Müller, M. R. Müller, and R. König, Colloid Polym. Sci. **260**, 444 (1982).
[19] A. Grabbe and R. G. Horn, J. Colloid Interface Sci. **157**, 375 (1993).
[20] J.-P. Chapel, Langmuir **10**, 4237 (1994).
[21] J. Davoust, P. F. Devaux, and L. Leger, EMBO J. **1**, 1233 (1982).
[22] A. van Blaaderen, J. Peetermans, G. Maret, and J. K. G. Dhont, J. Chem. Phys. **96**, 4591 (1992).
[23] A. Imhof, A. van Blaaderen, G. Maret, J. Mellema, and J. K. G. Dhont, J. Chem. Phys. **100**, 2170 (1994).
[24] W. Schärtl and H. Sillescu, J. Stat. Phys. **77**, 1007 (1994).
[25] W. G. Hoover and F. H. Ree, J. Chem. Phys. **49**, 3609 (1968).
[26] H. N. W. Lekkerkerker and A. Stroobants, Physica A **195**, 387 (1993).
[27] W. C. K. Poon and P. B. Warren, Europhys. Lett. **28**, 513 (1994).
[28] P. N. Pusey and W. van Megen, Phys. Rev. Lett. **59**, 2083 (1987).
[29] W. van Megen and S. M. Underwood, J. Chem. Phys. **91**, 552 (1989).
[30] B. Cichocki and B. U. Felderhof, J. Chem. Phys. **89**, 3705 (1988).
[31] W. van Megen and S. M. Underwood, Phys. Rev. E **49**, 4206 (1994).
[32] M. Venkatesan, C. S. Hirtzel, and R. Rajagopalan, J. Chem. Phys. **82**, 5685 (1985).
[33] B. Cichocki and B. U. Felderhof, J. Chem. Phys. **94**, 563 (1991).
[34] M. Medina-Noyola, Phys. Rev. Lett. **60**, 2705 (1988).
[35] I. C. Kim and S. Torquato, J. Chem. Phys. **96**, 1498 (1992).